

# Utilising SMES-FCL to improve the transient behaviour of a doubly fed induction generator DC wind system

□

**Abstract**—Wind energy is seen as one of the main pillars of renewable energy. However, the intermittent nature of these sources still poses as a major challenge. Moreover, sensitivity to grid faults and response to load changes are also main concerns.

Superconducting devices have been introduced to solve grid faults and energy storage problems associated with renewable energy sources. Nevertheless, the cost of superconducting materials was still a major drawback for their application in power grids.

In this paper, a novel power electronics circuit is used to connect the superconducting magnetic energy storage (SMES) to a DC system based on a doubly fed induction generator wind turbine. The proposed system merges energy storage function and the fault current limiting function into one device which is referred to as SMES-FCL in this paper.

The role played by the SMES-FCL is studied under various scenarios that may affect the whole system. The study of the system is carried in MATLAB/SIMULINK where the system is simulated in standalone and grid-connected modes. In the end, the proposed SMES-FCL control circuit is tested in a small-scale DC system experimentally.

**Index Terms**—DFIG wind turbines, fault current limitation, DC systems, Superconducting, energy storage.

## I. INTRODUCTION

The DFIG based wind turbines have many advantages over other wind turbine generators. They offer decoupled control of the active and reactive power and have partial rated converters which reduce cost and losses compared to other wind turbines [1], [2]. They can be used effectively to supply loads in remote areas as a standalone generator [3]. DFIGs have been used widely in AC systems with about 85 % of the total market share in 2008 [4].

Due to these outstanding features, DFIG wind turbines have been started to be connected to DC grids [5], [6]. The most common topology used to connect the DFIG to a DC bus is through an uncontrolled power converter. This is done by connecting the stator to the DC bus while connecting the rotor to the same bus using the rotor side converter [7]. This topology

benefits from having full control over the voltage and frequency of the generator. The main drawback of this topology is that it has high torque ripples and that the harmonics in stator currents appear due to the commutation of the stator diode rectifier. These problems have been solved by various control techniques. For example, in [8] a new control scheme is tested based on resonant and proportional-integrals controllers to reduce the torque ripples. In [9], another solution was offered to count these problems. Controlling sinusoidal stator currents directly without using voltage sensors have been used and tested experimentally to reduce the current harmonics.

Despite the outstanding advantages of the DFIG based wind turbines, during system disturbances the high currents induced in the stator and rotor may damage the converter. Trying to solve this problem by disconnecting the generator is not applicable for standalone microgrids, as it can interrupt the power delivery to critical loads. Also, losing high power generation in normal grids will affect system stability.

Generally, faults in DC systems are more severe than in AC systems. The DC fault amplitude depends on the type and location of the fault. As the resistance of the DC line is small and the fault can be fed from both the sources and capacitors, the fault currents might be catastrophic [10], [11]. With regards protection devices, normal circuit breakers which depends on the zero-crossing trip can't be used in DC grids. Instead, it uses fuses and special type circuit breakers like moulded-case, isolated-case which are typically in low voltage DC grids [12] or hybrid DC circuit breakers in HVDC systems [13].

Superconducting devices are considered to be promising candidates for solving many power grids problems. As an energy storage device, superconducting magnetic energy storage (SMES) devices have a high-power density, fast response time, high charging and discharging efficiency [14], [15] which makes it perfect for smoothing the output from wind power generation units [16], [17]. In addition to that, SFCL can be used in DFIG wind turbines- a switch type fault current limiter (STFCL) is connected in series with the DFIG stator side to limit fault currents in [18]. While in [19], a switchable resistive-type fault current limiter (SRFCL) was proposed and connected to the DC link of the DFIG unit to limit the rotor transient overcurrent. A single-phase bridge type FCL (BFCL) in [20] was compared to the series dynamic braking resistors in improving the transient stability of the DFIG during grid faults.

□

The idea of integrating fault current limitation function into a SMES has been proposed recently for applications in AC grids [21], [22], [23]. The superconducting coil (SC) can be connected in parallel or series to the DC-link capacitor of a DFIG converter. This type of connection can affect the system performance during faults because of the large inductance inserted and the SMES might lose its stored energy during the fault periods. In addition, connecting the SC into the rotor side converter or DC link requires one SC per each wind turbine, which will not be a very economically feasible solution with wind farms consisting of many wind turbine units.

A new technique proposed to limit faults in DC systems has been described in [24], which uses the entire SC coil in energy storage function under normal operating conditions and only a small part of the coils as a fault current limiter during fault conditions. In addition to using one device to perform two functions, this method avoids the disadvantage of the recovery period of the superconducting fault current limiter as it can be isolated from the circuit after the fault clearance, as will be detailed in section III.

This paper introduces the SMES-FCL circuit to improve the transient stability of the DFIG-DC system during different operating and fault conditions. The feasibility of supporting the loads in case of a voltage drop at the generator terminals is studied in addition to the fault current limitation function under different fault scenarios. This study was conducted in MATLAB/SIMULINK. To further investigate the behaviour of the proposed circuit and control method, a small-scale DC system was built and tested in the lab.

## II. SYSTEM DESCRIPTION

The system under test includes a DFIG-based wind turbine generator. The stator of the DFIG is connected to a three-phase diode rectifier and then to the DC bus. The rotor of the machine is connected to a voltage source converter (VSC) and then to the DC bus. The DC-system is connected to an AC grid to simulate the grid-connected mode. The AC grid model is used from the MATLAB/ Simulink library.

Fig 1 illustrates the circuit diagram of the system. The wind turbine generator has a rated power of 0.3 MW and voltage of 575 V. The transformer is a Y/D connection with 575-1350 V turns ratio. A 0.1 MW AC load is connected to the AC side

while the DC load is represented by a 10  $\Omega$  resistor connected to the DC line.

To focus on the behaviour of the DFIG with the proposed SMES-FCL, the system is represented by the DFIG-based wind turbine as the only generation unit. A detailed description for each part with its control algorithms is stated in the following section.

### A. The DFIG-based wind turbine system

The integration of the DFIG based wind turbines to DC grids have been introduced in the literature with different connection schemes [25], [26]. The topology used in this paper is connecting the stator windings to the DC bus using a three-phase diode bridge with the rotor connected also to the DC bus via a voltage source converter [7], [27]. The stator voltage and frequency are controlled using the rotor currents.

The voltage equations for the generator in the d-q reference frame are given as:

$$v_{ds} = R_s i_{ds} - \omega_s \lambda_{qs} + \frac{d\lambda_{ds}}{dt} \quad (1)$$

$$v_{qs} = R_s i_{qs} + \omega_s \lambda_{ds} + \frac{d\lambda_{qs}}{dt} \quad (2)$$

$$v_{dr} = R_r i_{dr} - (\omega_s - \omega_r) \lambda_{qr} + \frac{d\lambda_{dr}}{dt} \quad (3)$$

$$v_{qr} = R_r i_{qr} + (\omega_s - \omega_r) \lambda_{dr} + \frac{d\lambda_{qr}}{dt} \quad (4)$$

where:  $\lambda$  is the flux linkage,  $\omega$  is the angular frequency, R is the resistance per phase and s and r subscripts referring to stator and rotor. The flux linkage equations can be written as:

$$\lambda_{ds} = L_s i_{ds} + L_m i_{dr} \quad (5)$$

$$\lambda_{qs} = L_s i_{qs} + L_m i_{qr} \quad (6)$$

$$\lambda_{dr} = L_m i_{ds} + L_r i_{dr} \quad (7)$$

$$\lambda_{qr} = L_m i_{qs} + L_r i_{qr} \quad (8)$$

Choosing the synchronous rotating  $d$ - $q$  reference frame results in aligning the stator flux on the  $d$ -axis while setting its component on the  $q$ -axis to zero. Thus, the  $d$ - $q$  stator currents can be written as:

$$i_{ds} = \frac{(\lambda_{ds} - L_m i_{dr})}{L_s} \quad (9)$$

$$i_{qs} = (-L_m i_{qr}) / L_s \quad (10)$$

Simple vector control is used to adjust the active and reactive control loops [5]. The  $q$ -axis rotor current is used to control the

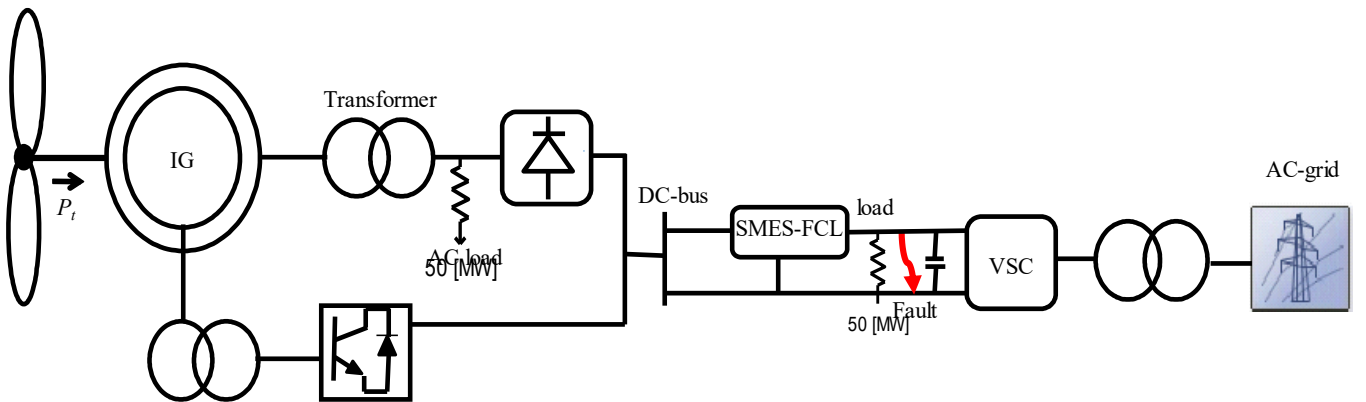


Fig.1.System configuration

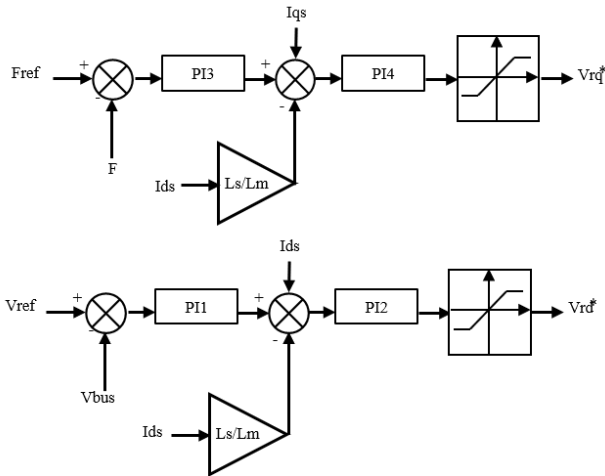


Fig. 2. Control of the RSC

frequency of the stator while the d-axis rotor current is used to control the DC voltage. Fig. 2 summarizes the control scheme of the rotor side converter. As shown on this figure, two PI loops are used to estimate each of the direct and quadrature reference voltages of the rotor. Then, they are transferred to the *abc* frame again to produce the gate signals for the rotor side converter. A phase locked loop is used to align the stator voltages to the right phase.

### A. SMES-FCL circuit

The SMES-FCL can be directly connected to the DC system. Fig. 3 shows the detailed structure of the SMES-FCL system and the operation modes. It contains two main IGBTs switches ( $Q_1$  &  $Q_2$ ) and two main diodes ( $D_1$  &  $D_2$ ). The idea of using the SMES as a two functional device depends on using the whole superconducting coil (SC) to store the energy in the normal operation mode. This includes charging, discharging and standby modes. One part of the SMES coils is separated and used as a superconducting FCL. This can be seen in Fig. 3 where the SMES coil is divided into two parts which are referred to as  $SC_1$  and  $SC_2$ . Both are used as energy storage coils whilst only  $SC_2$  is used as a fault current limiter.  $SC_1$  is isolated during fault conditions to reduce heat losses and to allow it to keep its stored energy.

### III. SYSTEM OPERATION

The proposed SMES-FCL circuit is connected to the DC-bus and tested to perform the two functions of energy storage and fault current limitation. When the current in the main DC line is less than the maximum set value ( $I_{set}$ ), the system operates as a normal operation or energy storage mode. During this mode,  $Q_4$  and  $Q_6$  are kept on,  $Q_3$  and  $Q_5$  are kept off whilst the two diodes  $D_3$  and  $D_4$  are forward and reverse biased respectively.

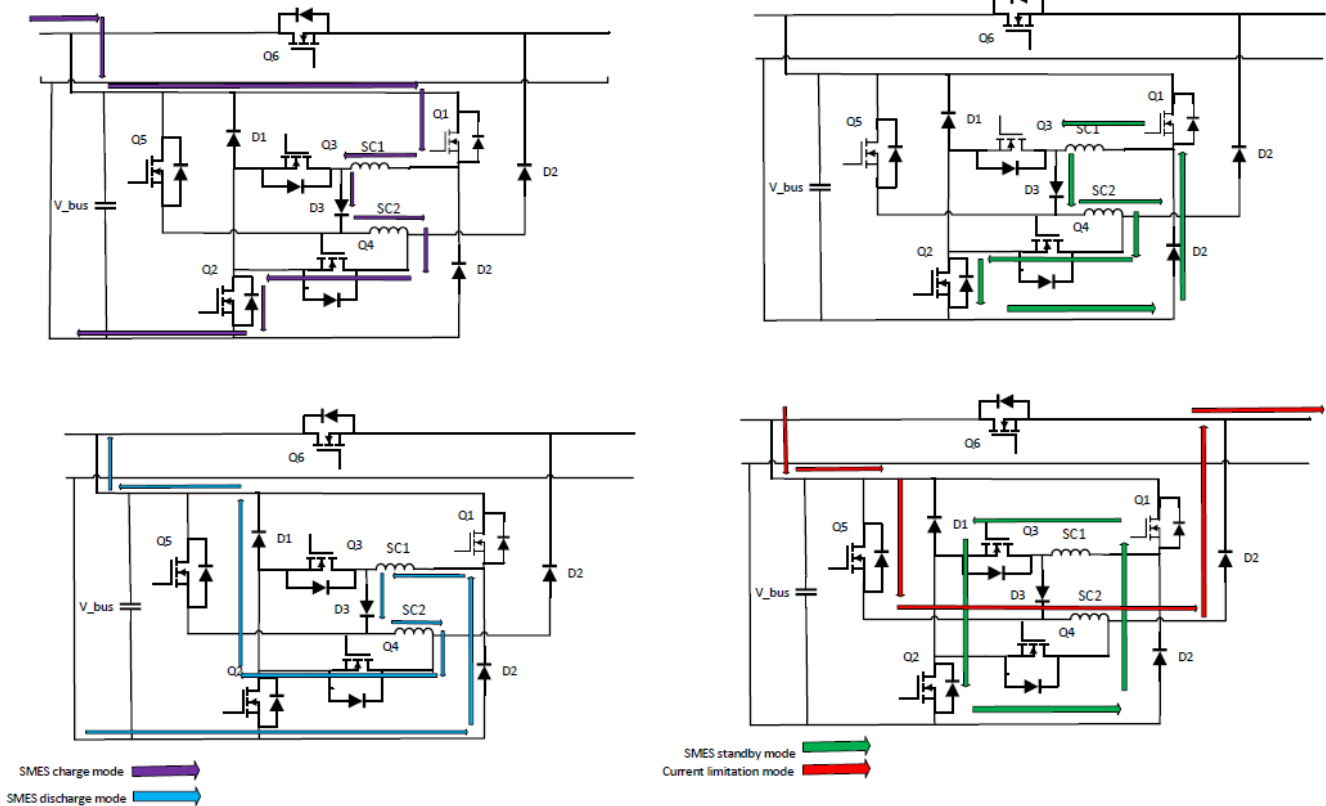


Fig. 3. SMES-FCL circuit and operation modes

TABLE 1  
Switching sequence

| Operation mode          | Condition                         | Q <sub>1</sub> | Q <sub>2</sub> | Q <sub>3</sub> | Q <sub>4</sub> | Q <sub>5</sub> | Q <sub>6</sub> | D <sub>1</sub> , D <sub>4</sub> | D <sub>2</sub> , D <sub>3</sub> |
|-------------------------|-----------------------------------|----------------|----------------|----------------|----------------|----------------|----------------|---------------------------------|---------------------------------|
| Energy storage modes    | I <sub>DC</sub> <I <sub>set</sub> | On/off         | On/off         | off            | On             | off            | On             | off                             | On                              |
| Current limitation mode | I <sub>DC</sub> >I <sub>set</sub> | On             | off            | On             | off            | On             | off            | on                              | off                             |

The two main IGBTs (Q<sub>1</sub>& Q<sub>2</sub>) are turned ON or OFF according to the voltage on the DC line in the connection point. A reference value is set to 1150 V, which equals the average DC voltage at normal operation mode. When the voltage is higher than the reference value, the two switches are ON charging the coil. When the voltage is less than the reference, Q<sub>1</sub> and Q<sub>2</sub> are off whilst the two diodes D<sub>1</sub> and D<sub>2</sub> are forward biased to discharge the coil to support the system. If the voltage is the same as the reference value, the coil keeps its energy by circulating it in Q<sub>2</sub> and D<sub>2</sub> which represents the standby mode. The DC chopper control is performed using a program which calculates the duty cycles of the switches and then the pulses are generated using the pulse width modulation techniques. Applying Kirchhoff's voltage law (KVL) at Fig. 3, the DC bus voltage can be given as:

$$V = L \frac{di(t)}{dt} + I(t)R_t \quad (11)$$

Where V is the DC bus voltage, L is the total inductance of the SC, I(t) is the SMES current and R<sub>t</sub> is the total resistance including the self-resistance of the SC and the total resistance of the power electronic switches.

Solving this equation and assuming the initial current in the SC is I<sub>0</sub>, the SMES current at any instant can be expressed as [28]:

$$I(t) = I_0 \exp\left(-\frac{R_t t}{L}\right) + \frac{V}{R_t} [1 - \exp\left(-\frac{R_t t}{L}\right)] \quad (12)$$

During the discharging process, the SMES current will decrease to support the system voltage with a time constant which equals to L/R<sub>t</sub>.

When the main system current increases to the fault level, Q<sub>6</sub> is opened whilst Q<sub>5</sub> is closed to allow the high system current to pass through SC<sub>2</sub>. Once the current reaches the critical value of the coil, SC<sub>2</sub> quenches and introduces resistance to the main system during the fault. The resistance of the superconducting materials (R<sub>SFCL</sub>) increases to high values according to the value of the current and temperature based on the following equation:

$$R_{SFCL} = \begin{cases} 0 & (J < J_c, T < T_c) \\ f\left(\frac{E_c}{J_c(T)} \left(\frac{J}{J_c(T)}\right)^{N-1}\right) & (J > J_c, T < T_c) \\ f(T) & (T > T_c) \end{cases} \quad (13)$$

Where J<sub>c</sub> and T<sub>c</sub> are the critical current density and the critical temperature of the superconducting material. E<sub>c</sub> is the critical electric field which represents the maximum endurable voltage per unit length. The N constant depends on the type of the superconducting material. From Eq (13), the operation zones of the superconducting material are divided into three regions, the zero resistance (superconducting), the flux flow and the normal resistance zones. The second zone is

neglected in this simulation study and the two other zones are considered based on the current value. More details about superconducting material's behaviour can be found in [29], [30]. A major concern during this period is to isolate the rest of the SC (SC<sub>1</sub>) to keep its energy. This is done by opening Q<sub>4</sub> and closing Q<sub>3</sub> and Q<sub>1</sub> with D<sub>1</sub> forward biased to allow the stored current to circulate. This sequence can be summarized as in TABLE 1. The settings for the SMES-FCL system are determined based on the operation current of the main system. The initial value of the SMES current is 150 A and the value which activates the fault current limitation mode (I<sub>set</sub>) is 300 A. The limitation effect is determined mainly by the value of the fault current limiter resistance, which depends on the number of pancakes which operate as a fault current limiter in addition to energy storage. As the resistance of the SC<sub>2</sub> will be high compared to its inductance, the energy stored on the SC<sub>2</sub> will be dissipated during the current limitation process.

#### IV. SYSTEM PARAMETERS

The parameters of the SMES coil are determined by the energy capacity required by the system. In this system, the generator's rated power is 0.5 MW and the AC load is 0.1 MW, which means supplying the DC load for 0.5 sec at rated power requires 0.2 MJ energy. On the other hand, the operating current of the SMES is chosen to match the DC current of the main system. The energy stored on the SC can be calculated from:

$$E = \frac{1}{2} L I_{smes}^2 \quad (14)$$

Based on this equation and with an operating current of 150 A, the inductance of the coil is 10 H. As the YBCO superconducting tapes have better characteristics than other high-temperature superconducting materials [31] for high field applications such as SMES, YBCO tapes are used for this study. The critical current of a tape chosen in this study is 300 A at 77 K, self-field. With a 40 μm thickness copper stabilizer and a tape width of 4mm, the resistance of the tape at room temperature is 0.12 Ω/m [32]. A current limitation resistance of 5 Ω is calculated to be suitable for the studied system in order not to reduce the current during faults to very low values and prevent the protection system from detecting the fault. Thus, a total length of 40 m is required for the fault current limiting coils, resulting in a few mH inductance value based on the winding configuration.

#### V. SIMULATION RESULTS AND DISCUSSION

To study the effectiveness of the SMES-FCL to act as an energy storage device and as a fault current limiter, several scenarios are simulated. As the microgrids can operate either in standalone or connected modes, these two cases are studied and the ability of the SMES-FCL to support the load and limit fault currents is investigated.

A. Stand-alone mode

In this mode, the DFIG supplies the AC and DC loads alone and there is no connection with the AC grid. This mode is chosen to illustrate how the SMES can support the load in case of a voltage drop on the generation side and also to remove the ripples from the power output of the wind generator with variable wind speed. First, a variable wind speed is applied to the wind turbine generator and the power at the DC load is monitored with and without using the SMES-FCL. The current setting for the fault current limiter mode should be chosen as that the set value is higher than the maximum rated current with the highest wind speed taking into account of a safety margin. It is clear from Fig. 4 that the SMES-FCL can effectively smooth the output power at the load terminals with charging and discharging the SMES coil. The only function used in this case is the energy storage function. Fig. 5 illustrates the wind speed profile applied to the wind turbine model and the charging and discharging process of the SMES current responding to the increase or decrease in power output.

The ability of the SMES-FCL to support the load during a voltage drop at the generator terminals is studied in the second scenario. A voltage drop at the generator terminals for a period of 200 milliseconds is applied from the 15 second with the DC

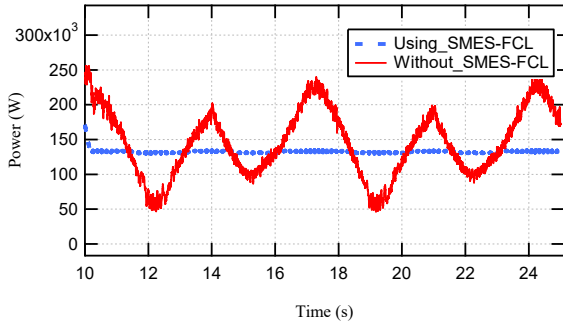


Fig. 4. Load power without and with using the SMES-FCL

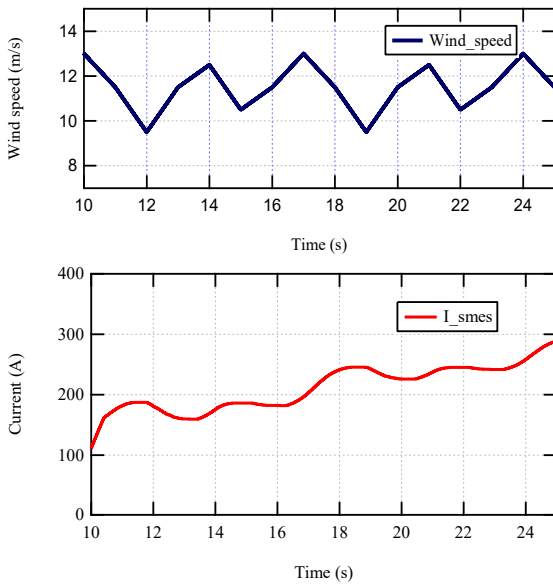


Fig.5. The wind speed profile and the SMES-current with variable wind speed operation

load voltage and current being monitored. Figs. 6 and 7 illustrate the current and voltage at the DC load terminals during the voltage drop scenario. The SMES-FCL has been able to effectively compensate the voltage drop and to support the load voltage and current during this period. The drop in the current at the load terminals reduced from about 15 A to only 2 A. While the maximum drop in the voltage reduced from 150 V to about 25 V when using SMES-FCL. Moreover, the suggested technique has enhanced the voltage profile after the end of the voltage drop period. The SMES coil current shown in Fig.8 illustrates the discharging process during the voltage drop period to support the load power.

The third scenario with the stand-alone mode is to apply a DC fault (pole to pole) from 16 to 16.1s on the DC line and study the fault current limitation ability of the proposed device. The DC fault is created by an ideal switch in the simulation. The DC line current is shown in Fig. 9. The maximum current is observed to be more than 1200 A without using the SMES-FCL and is limited to about 300A after using it. Moreover, using the SMES alone helps in improving the post value behaviour and resuming stability but with a small limitation effect at the start of the fault.

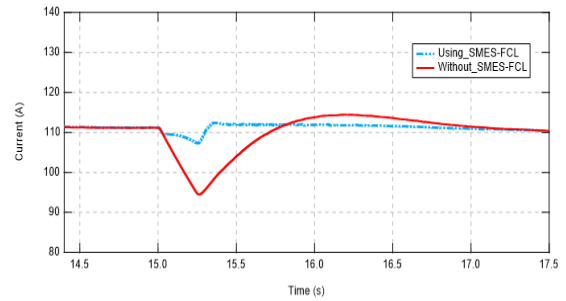


Fig. 6. Load current without and with using the SMES-FCL

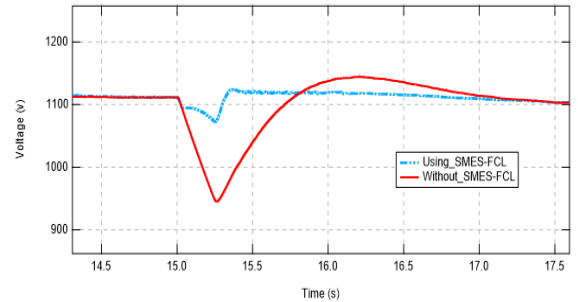


Fig. 7. Load voltage without and with using the SMES-FCL

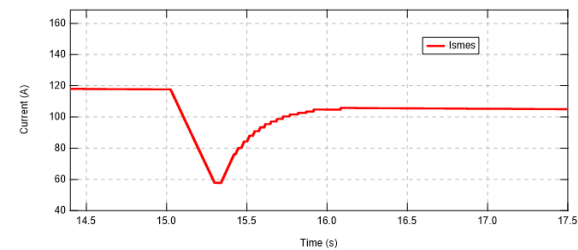


Fig. 8. SMES-current during voltage drop scenario.

The voltage drop at the generator DC side also decreased by using the SMES-FCL. In Fig.10 the DC voltage increased from zero to ~550 V during the fault inception. Then the voltage is increased to about 750 V before returning to pre-fault value after 1.5 seconds only compared to 5 seconds without using the SMES-FCL. Using the SMES without integrating the fault current limiter function helps the voltage return to stability by regaining the voltage of the DC bus after the fault period. In addition, reducing the voltage value during the fault period to an average of 0.6 pu using the SMES-FCL improves the voltage profile to comply with most grid codes [33]. As the pole-to-pole DC fault is a severe fault, the mechanical speed and the rotor currents are monitored in this scenario. Fig. 11 shows the rotor speed during the DC fault with the SMES-FCL, with only SMES and without any of them. The increase in the generator speed is reduced to have a peak value of 1.5 pu using the SMES and 1.3 pu using the SMES-FCL from a prospective value of 1.62 pu otherwise. In addition, the generator resumes stable operation in 2.5 seconds compared with 6 seconds without the SMES-FCL. Fig. 12 illustrates the enhancement in the rotor currents using the proposed scheme. The prospective rotor currents drop to zero at the end of the fault period, while this drop in the current value is clearly reduced using the SMES-FCL and the rotor currents returned to the pre-fault value after less than one second.

### B. Grid-connected mode:

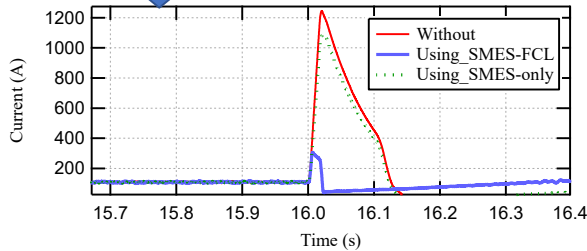
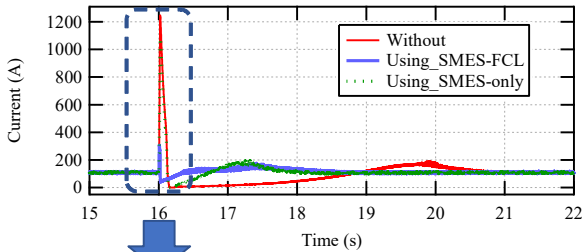


Fig. 9. DC current during a DC fault in stand-alone mode

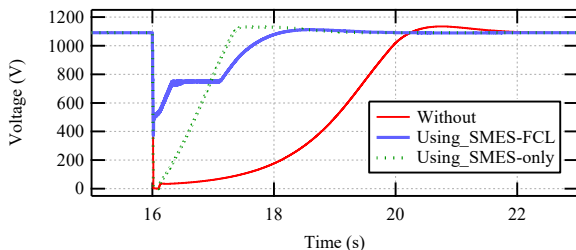


Fig. 10. DC voltage during a DC fault in stand-alone mode

As the DC system is connected to the AC grid, the fault types can be both AC and DC. A DC fault would be more harmful to

the system as with the low inductances the current increases to a very high value [34]. The current limitation during the connected mode is investigated by applying the fault on the DC bus for a period of 100 ms. The current on the DC bus is as shown in Fig.13 where the limitation is very clear. The fault current is reduced to about 75% from the prospective value when using the SMES-FCL.

The second parameter to be considered is the DC bus voltage. It is very important to keep the voltage drop in suitable limits to comply with grid codes and prevent the generator from tripping during the fault [33]. During faults, the voltage drop at the generator terminals must be higher than the indicated limits to prevent the generator from tripping during faults. As shown in Fig. 14, the voltage during the fault period increased from zero to 750 V with using the SMES-FCL. However, after the fault period, the voltage still has some transients and needs time to return to stability. To enhance the behaviour after the fault, further coordination with the AC grid converter is required. A three phase to ground short circuit fault is applied at the AC grid side for 100 milliseconds starting from the second 13. The DC line current and DC voltage during this scenario are shown in Fig. 15 and Fig. 16 respectively. It can be seen from these figures that the value of the current does not show a large

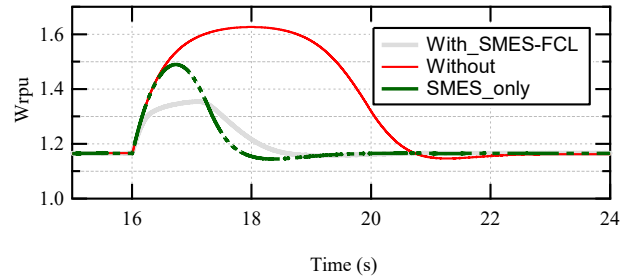


Fig. 11. Generator speed during a DC fault in stand-alone mode

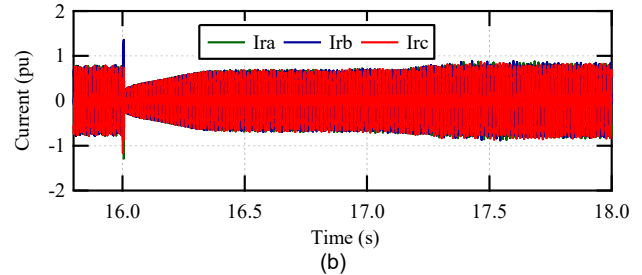
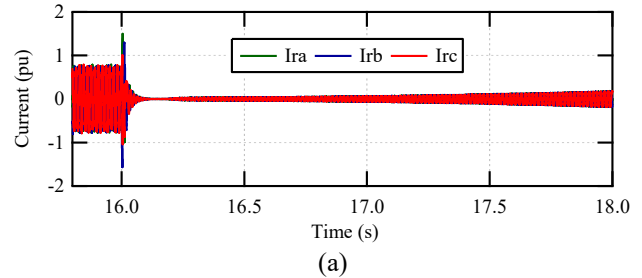


Fig. 12. Rotor currents during a DC fault in stand-alone mode (a) without SMES-FCL. (b) Using SMES-FCL

increase which means the current limitation function is not used in this case. The SMES-FCL helps the system to restore to its pre fault value which is clear from the voltage profile in Fig. 16. From this section, it can be concluded that the SMES-FCL can be used in both standalone and grid-connected modes. However, the benefits in the standalone mode are more significant especially in compensating the voltage drop and supporting the load.

### C. Discussion

Integrating the fault current limiting function into the SMES systems requires additional power electronics and control circuits. A comparison with other fault current limiting

techniques is needed to evaluate the effectiveness of the SMES-FCL system. Non-superconducting technologies used in DC systems are the major competitors to the superconducting-based fault current limiters.

In [35], a new type of non-superconducting fault current limiter (NFCL) is used to limit fault currents in a DC system. It mainly consists of a permanent magnet, iron core and two coils. The first coil is connected to the DC circuit and the other is responsible for current limitation. The iron core saturation state is used to limit fault currents. This new NFCL achieves a good current limitation compared to traditional fault current limiters. It can limit the current in less than 5 milliseconds. However, the operation principle of this type depends on coordination with a specific circuit breaker which limits its integration applicability to existing systems. In addition, the iron core increases the size and makes the overall device bulky. Another study on the NFCL connected to the DC line is presented in [36]. A capacitor is charged during fault periods and then returns this charged energy to the system after fault elimination. It consists of an isolating transformer, reactor, resistors, power electronic switches and the capacitor. This FCL aimed to reduce currents at the AC side which is connected via a rectifier to the DC bus and the FCL side. This method is effective in limiting faults in the AC side not the DC side.

Comparing the SMES-FCL with these two examples proves that the SMES-FCL could achieve good current limitation in a few milliseconds. It can be adjusted and integrated with any type of DC system with a suitable number of coils required for current limitation and adapting the settings of the control system.

## VI. THE EXPERIMENTAL TEST OF THE SMES-FCL

The proposed circuit of the SMES-FCL is tested in a small-scale DC system. The system consists of a controllable DC source, connected to a DC load represented by a resistor. The connection diagram and the experiment set up are illustrated in Fig. 17. The parameters of the components used in the SMES-FCL test are listed in TABLE 2. The used SMES coil can store up to 30 J at 20 A operating current. The SMES coil plays a major role in this experiment as it is used to support the voltage and the current delivered to the load with different changes on the supply side. The  $E-J$  characteristics of the used SMES coil is illustrated in Fig. 18. When the current value reaches about 43 A, the voltage drop at the tape terminals is 0.1  $\mu\text{V}/\text{cm}$ . After this value, the voltage starts to increase with a high rate which means the tape is losing the superconductivity. The circuit is set to operate at 6 A and then the current increases to 10 A for about 13 seconds in the first tested scenario. This scenario represents a power increase in the generation side.

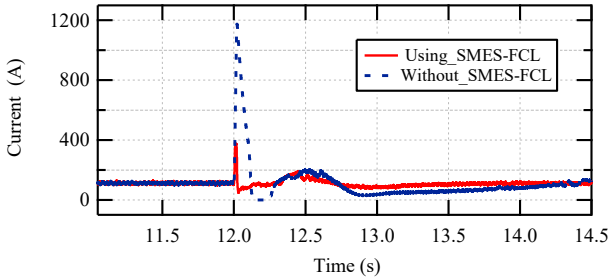


Fig. 13. DC current during a DC fault in connected mode

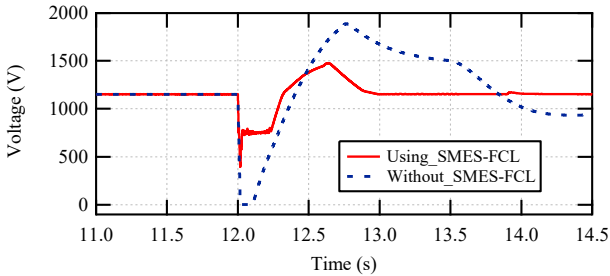


Fig. 14. DC voltage during a DC fault in connected mode

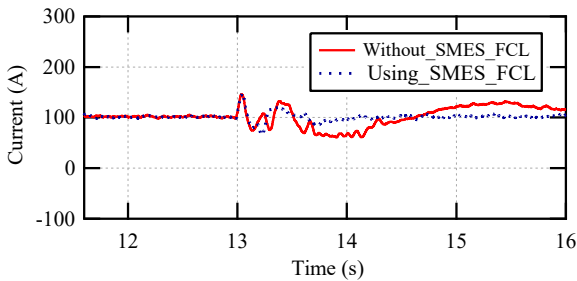


Fig. 15 DC current during a three-phase fault in the AC grid

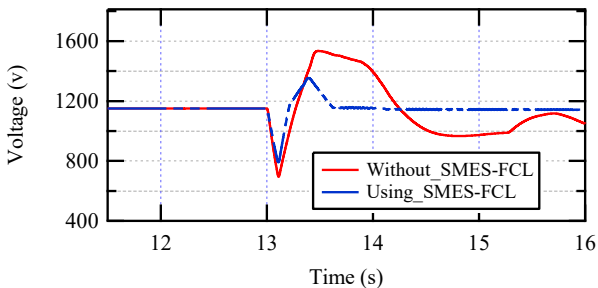


Fig. 16 DC voltage during a three-phase fault in the AC grid

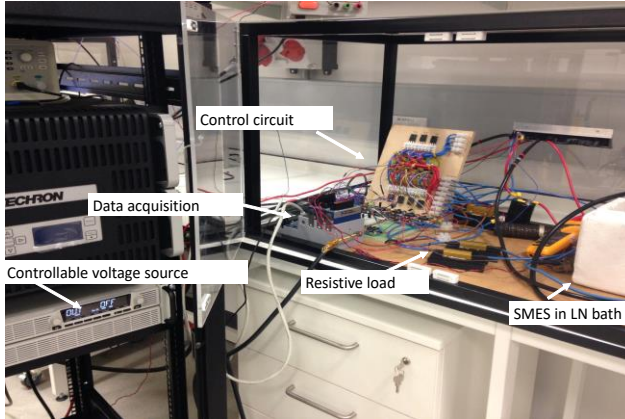
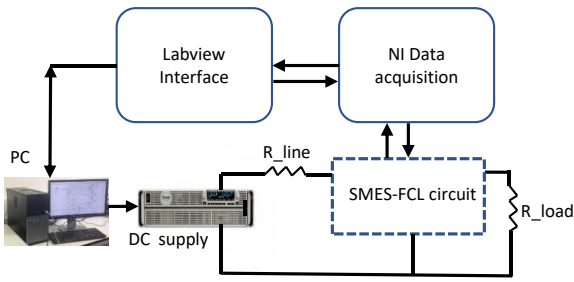


Fig. 17. The connection diagram and the experimental setup

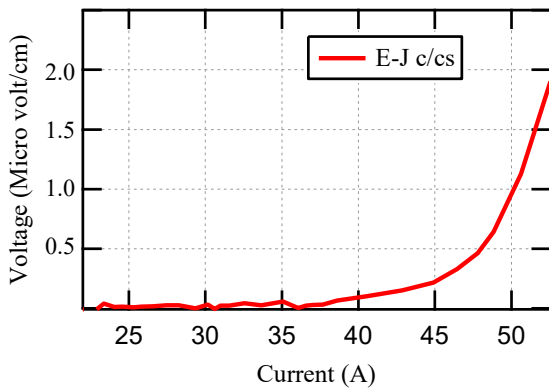


Fig. 18. E-J characteristics of the SMES coil

TABLE 2  
Components used in the experimental test

| Element                 | Number | Details   |
|-------------------------|--------|---|
| DC power supply         | 1      | TDK-Lambda GSP10-1000<br>10V/1000A  |
| $R_{line}$              | 1      | 0.27 $\Omega$ , 100W  |
| $R_{load}$              | 2      | 1 $\Omega$ , 50 W   |
| Capacitor               | 1      | 47000 $\mu$ F   |
| IGBTs                   | 7      | IKW40N120CS6, 40A   |
| Diodes                  | 4      | FFSB3065B-F085, 30A   |
| Data acquisition system | 1      | National instruments DAQ system   |
| SMES coil               | 1      | <ul style="list-style-type: none"> <li>2 pancakes coil</li> <li>Inner radius 45 mm and outer radius of 73 mm.</li> <li>The rated current is 33 A, and the critical current is 42 A</li> </ul> |
| Fault current limiter   | 1      | Emulated by a .05 $\Omega$ resistance in parallel with a power electronic switch  |

Fig.19 illustrates the voltage at the connection point under this scenario with and without connecting the SMES-FCL. The voltage during the current pulse reached 6.3 V and this value is reduced to about 5.1 V with using the SMES-FCL. In addition, the current delivered to the load is reduced from 10 A to 7.9 A with using the SMES-FCL as shown in Fig. 20. These results correspond to an enhancement in the voltage increase from 57.5 % to 27.5 % from the prospective value and the current increase was limited from 66.6% to 31.66 %. The charging process of the SMES coil during this case is clear in Fig. 21 where the current increased from zero to approximately 2.1 A during the increase in the source current. The second scenario is the

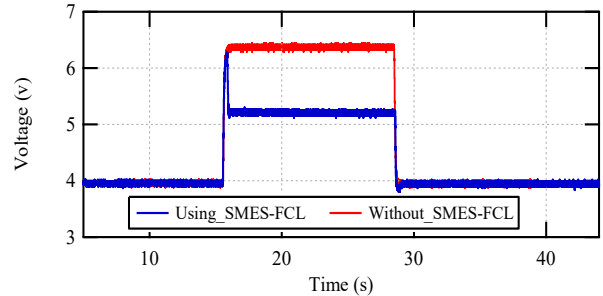


Fig.19. Connection point voltage with and without using the SMES-FCL during an increase in the source current.

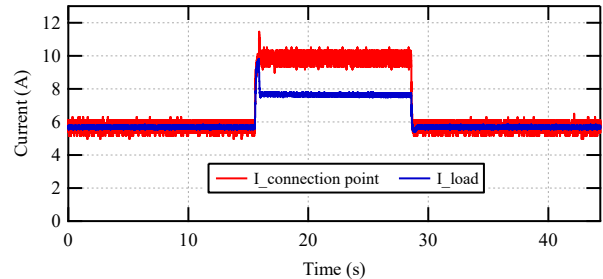


Fig.20. Currents of the connection point and the load during an increase in the source current

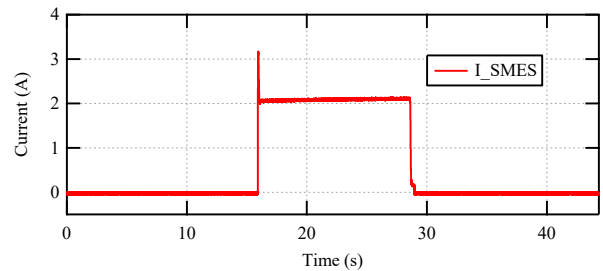


Fig. 21. SMES-coil current during an increase in the source current

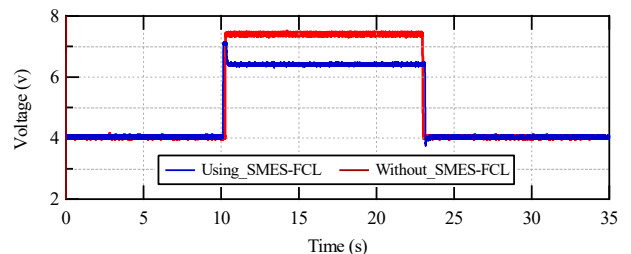


Fig. 22. Connection point voltage with and without using the SMES-FCL during an increase in the source voltage.

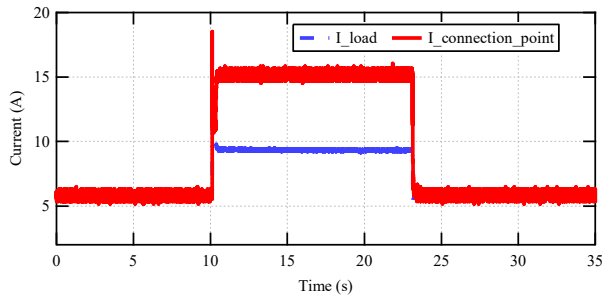


Fig.23. Currents of the connection point and the load during an increase in the source voltage

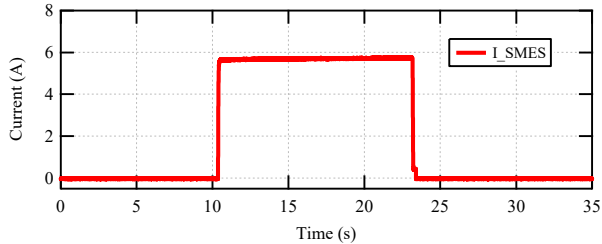


Fig.24. SMES-coil current during an increase in the source voltage

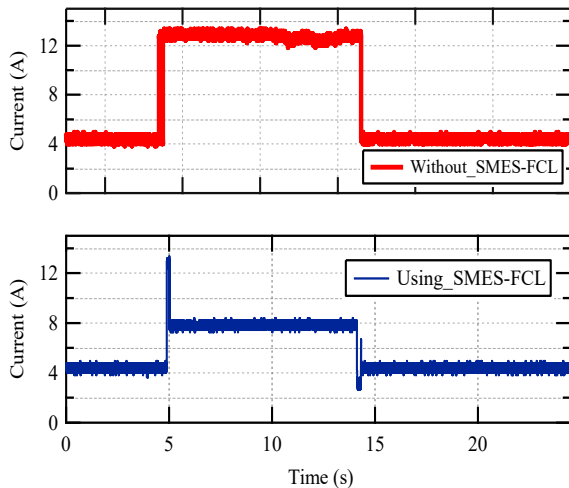


Fig.25. DC line current during the current limitation test

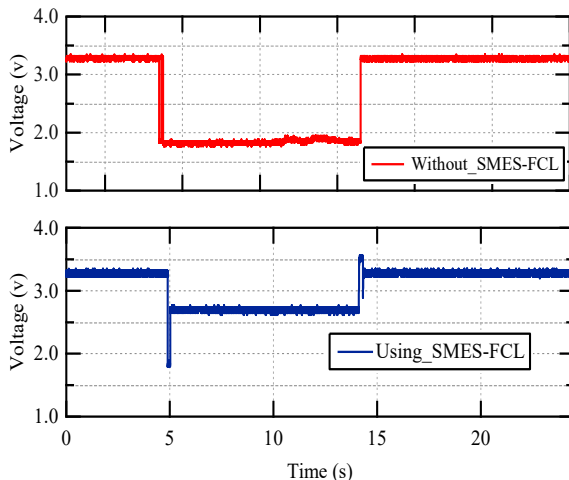


Fig.26. The connection point voltage during the current limitation test

increase in the source voltage from a normal value of 5 V to a pulse of 9 V for about 13 seconds to represent voltage disturbances. Fig. 22 and Fig. 23 illustrate the connection point voltage and the load current during this case. It is clear from the figures that connecting the SMES-FCL reduced voltage increase by 1 V which represents 25 % of the normal voltage value. In addition, the current at the load side is reduced from about 15.5 A to about 9.5 A with using the SMES-FCL. Fig. 24 shows the SMES coil current which is charged to near 6 A during the source voltage increasing period. During the first and the second scenarios, the reference voltage value is set to be 4 V at the connection point and the critical current is set to be 20 A to prevent the FCL mode activation. The third scenario is to test of the fault current limitation function. The fault case is emulated by increasing the circuit current to a value which is higher than the critical current setting value. The critical current value to activate the fault current limiter mode is set to be 7 A in this case. The source voltage is set to be 4 V to avoid high currents flowing into the circuit and the reference voltage value is 3.3 V at the connection point. Fig. 25 illustrates the current on the main DC line with and without using the SMES-FCL. The current is limited from 13 A to 8 A when using the SMES-FCL which represents percentage limitation of 38.5 % from the prospective value. Moreover, as shown in Fig. 26 the voltage at the connection point has a voltage drop of about 1.5 V, which represents 0.45 pu without the fault current limitation. This drop is reduced to about 0.6 V which represents 0.18 pu when using the SMES-FCL. The current and voltage instant peaks in the experimental results are mainly due to the time taken by current sensor to detect a fault and to send the switching signal to the control circuit.

## VII. COST AND INDUSTRIAL APPLICATIONS

In designing a superconducting magnet, the cost will be a major factor alongside the total efficiency. According to [37], the cost of the storage element in a SMES system can range from \$85 K to \$125 K per MJ, and the cost of the power-conversion system could be between \$150 and \$250 per kW [38]. Although these numbers are comparatively old, their wide range reflects the fact that the cost of a SMES system can be subject to many parameters. The capital cost includes the cost of all the components of the SMES system. The superconducting magnet and power conversion circuits are the two main components in the SMES system. The cost of the superconducting magnet changes with material types. Furthermore, the physical dimensions of the magnet, especially its total tape length, is the main factor affecting the cost of the magnet. The tape length, in turn, depends on the energy storage requirement and the design method of the coil. Superconducting coils form about 20-25 per cent of the total cost [39]. As an example, the cost of a REBCO tape is 140 \$/kA.m at temperature  $T = 30$  K and perpendicular  $B = 2$  T [40]. Although the price of HTS materials is still high, prices are showing an annual decline of about 10 per cent [38], which will increase the opportunities for the commercialization of SMES systems in the near future. Adding the fault current limitation function to the SMES system does not require additional magnet cost as it uses a part of the SMES magnet. The power converter interface

forms from 15 to 30 per cent of the total SMES system cost [39]. As the SMES-FCL requires more power electronic switches this value may increase based on the system rating and whether it is connected to an AC or DC system which requires less power conversion stages.

In summary, the SMES-FCL can play an important role in systems including intermittent renewable energy generation. It can replace the use of an individual energy storage system and a separate fault current limiter system. It is also very promising for applications where the size and weight are major concerns such as in electric aircraft and all-electric ships.

### VIII. CONCLUSION

In this paper, a new technique that uses SMES-FCL system has been introduced in DC systems. The SMES-FCL coil effectiveness has been tested with a microgrid containing DFIG-DC system. The SMES coil has been able to effectively smooth the output power of the wind turbine and support the load in case of a voltage drop at the generator terminals. With added power electronic switches and dedicated control algorithms, a portion of the same coil can be used as a superconducting fault current limiter. The portion of the coil is used to limit the fault current whilst the other part of the coil is isolated to avoid overheating during fault periods and to keep the stored energy stored. The suggested SMES-FCL has been able to effectively limit the fault current within a few milliseconds and enhancing the system performance during and after the fault period. This technique can be used to reduce the fault current levels and act as a backup to protection systems in case of any failure. The proposed system is tested in a small-scale lab experiment and has demonstrated its effective energy storage function and current limitation function. Adding more generation units to an existing system may require upgrading the protection system to higher values. By using the current limitation function, we can decrease the fault current magnitude to suit the old circuit breakers' ratings and avoid upgrading thereby saving costs.

### IX. ACKNOWLEDGMENT

Mariam Elshiekh wants to thank the Newton-Mosharafa fund program between the British council and the Egyptian government for funding her PhD scholarship at the University of Bath, UK.

### REFERENCES

- [1] S. Muller, M. Deicke and R. W. De Doncker, "Doubly fed induction generator systems for wind turbines," in *IEEE Industry Applications Magazine*, vol. 8, no. 3, pp. 26-33, May-June 2002. doi: 10.1109/2943.999610
- [2] J. John, F. Mwasilu, and J. Jung. "Doubly-fed induction generator based wind turbines: A comprehensive review of fault ride-through strategies." *Renewable and sustainable energy reviews* 45 (2015): 447-467.
- [3] A. B. Ataji, Y. Miura, T. Ise and H. Tanaka, "Direct Voltage Control With Slip Angle Estimation to Extend the Range of Supported Asymmetric Loads for Stand-Alone DFIG," in *IEEE Transactions on Power Electronics*, vol. 31, no. 2, pp. 1015-1025, Feb. 2016. doi: 10.1109/TPEL.2015.2414481
- [4] Goudarzi, Navid, and W. D. Zhu. "A review on the development of wind turbine generators across the world." *International Journal of Dynamics and Control* 1.2 (2013): 192-202.
- [5] B. Touaiti, M. Moujahed, H. Ben Azza, and M. Jemli. "Fault-tolerant VSI for stand-alone DFIG feeding an isolated DC load." *International Journal of Electronics* 105, no. 10 (2018): 1769-1784.
- [6] X. Yi and H. Nian, "Novel DC grid connection topology and control strategy for DFIG-based wind power generation system," *2013 International Conference on Electrical Machines and Systems (ICEMS)*, Busan, 2013, pp. 223-228. doi: 10.1109/ICEMS.2013.6754426
- [7] M. F. Iacchetti, G. D. Marques and R. Perini, "Operation and design issues of a doubly fed induction generator stator connected to a dc net by a diode rectifier," in *IET Electric Power Applications*, vol. 8, no. 8, pp. 310-319, September 2014. doi: 10.1049/iet-epa.2013.0405
- [8] G. D. Marques and M. F. Iacchetti, "Minimization of Torque Ripple in the DFIG-DC System Via Predictive Delay Compensation," in *IEEE Transactions on Industrial Electronics*, vol. 65, no. 1, pp. 103-113, Jan. 2018. doi: 10.1109/TIE.2017.2716860.
- [9] C. Wu and H. Nian, "Sinusoidal Current Operation of a DFIG-DC System Without Stator Voltage Sensors," in *IEEE Transactions on Industrial Electronics*, vol. 65, no. 8, pp. 6250-6258, Aug. 2018. doi: 10.1109/TIE.2017.2786259
- [10] J. Park and J. Candelaria, "Fault Detection and Isolation in Low-Voltage DC-Bus Microgrid System," in *IEEE Transactions on Power Delivery*, vol.28, no.2, pp.779-787, April 2013. doi: 10.1109/TPWRD.2013.2243478
- [11] P. Ruffing, N. Collath, C. Brantl and A. Schnettler, "DC Fault Control and High-Speed Switch Design for an HVDC Network Protection Based on Fault-Blocking Converters," *IEEE transactions on power delivery*, vol. 34, no. 1, pp. 397- 406, Feb 2019. doi: 10.1109/TPWRD.2018.2883861
- [12] D. Salomonsson, L. Soder and A. Sannino, "Protection of Low-Voltage DC Microgrids," in *IEEE Transactions on Power Delivery*, vol. 24, no. 3, pp. 1045-1053, July 2009. doi: 10.1109/TPWRD.2009.2016622
- [13] X. Pei, O. Cwikowski, A. C. Smith and M. Barnes, "Design and Experimental Tests of a Superconducting Hybrid DC Circuit Breaker," in *IEEE Transactions on Applied Superconductivity*, vol. 28, no. 3, pp. 1-5, April 2018, Art no. 5000205. doi: 10.1109/TASC.2018.2793226
- [14] H. Alafnan *et al.*, "Stability Improvement of DC Power Systems in an All-Electric Ship Using Hybrid SMES/Battery," in *IEEE Transactions on Applied Superconductivity*, vol. 28, no. 3, pp. 1-6, April 2018, Art no. 5700306. doi: 10.1109/TASC.2018.2794472
- [15] M. E. Elshiekh, D.-E. A. Mansour, M. Zhang, W. Yuan, H. Wang and M. Xie, "New Technique for Using SMES to Limit Fault Currents in Wind Farm Power Systems," *IEEE Transactions on Applied Superconductivity*, vol. 28, no. 4, p. 5602005, June 2018. doi: 10.1109/TASC.2018.2810512
- [16] H. M. Hasanien, "A Set-Membership Affine Projection Algorithm-Based Adaptive-Controlled SMES Units for Wind Farms Output Power Smoothing," in *IEEE Transactions on*

- Sustainable Energy*, vol. 5, no. 4, pp. 1226-1233, Oct. 2014. doi: 10.1109/TSTE.2014.2340471
- [17] Changjin Liu, Changsheng Hu, Xiao Li, Yi Chen, Min Chen and Dehong Xu, "Applying SMES to smooth short-term power [1] in wind farms," *2008 34th Annual Conference of IEEE Industrial Electronics*, Orlando, FL, 2008, pp. 3352-3357. doi: 10.1109/IECON.2008.4758498
- [18] W. Guo. et. al, "LVRT Capability Enhancement of DFIG With Switch-Type Fault Current Limiter," *IEEE Transactions on Industrial Electronics*, vol. 62, no. 1, pp. 332-342, 2015.
- [19] Naderi, Seyed Behzad, et al. "Low voltage ride-through enhancement of DFIG-based wind turbine using DC link switchable resistive type fault current limiter." *International Journal of Electrical Power & Energy Systems* 86 (2017): 104-119.
- [20] G. Rashid and M. H. Ali, "Transient stability enhancement of doubly fed induction machine-based wind generator by bridge-type fault current limiter," *IEEE Transactions on Energy Conversion*, vol. 30, no. 3, pp. 939-947, 2015.
- [21] X. Xiao, R. Yang, X. Chen and Z. Zheng, "Integrated DFIG Protection With a Modified SMES-FCL Under Symmetrical and Asymmetrical Faults," in *IEEE Transactions on Applied Superconductivity*, vol. 28, no. 4, pp. 1-6, June 2018, Art no. 5400606. doi: 10.1109/TASC.2018.2802782
- [22] W. Guo, L. Xiao and S. Dai, "Enhancing Low-Voltage Ride-Through Capability and Smoothing Output Power of DFIG With a Superconducting Fault-Current Limiter–Magnetic Energy Storage System," *IEEE Transactions on Energy Conversion*, vol. 27, no. 2, pp. 277 - 295, June 2012. doi: 10.1109/TEC.2012.2187654.
- [23] I. Ngamroo and T. Karaipoom, "Improving Low-Voltage Ride-Through Performance and Alleviating Power Fluctuation of DFIG Wind Turbine in DC Microgrid by Optimal SMES With Fault Current Limiting Function," in *IEEE Transactions on Applied Superconductivity*, vol. 24, no. 5, pp. 1-5, Oct. 2014, Art no. 5700805. doi: 10.1109/TASC.2014.2333031
- [24] H. Alafnan. et. al., "Application of SMES-FCL in Electric Aircraft for Stability Improvement," *IEEE Transactions on Applied Superconductivity*, vol. 29, no. 5, pp. 1-6, August 2019. doi: 10.1109/TASC.2019.2905950
- [25] J. Li and K. Corzine, "A sensorless flux oriented control scheme for a DFIG connected to a DC link," *2015 Clemson University Power Systems Conference (PSC)*, Clemson, SC, 2015, pp. 1-5. doi: 10.1109/PSC.2015.7101696 5.
- [26] X. Wang, X. Cui, G. Tergemessova, Q. Liu, H. Zhang and J. Lai, "Behavior of responding to sudden change of standalone dc load supplied by a DFIG with different frequency in AC side," in *Asian Conference on Energy, Power and Transportation Electrification (ACEPT)*, Singapore, 2017.
- [27] R. Dev, and R. Kumar. "DC grid/bus tied DFIG based wind energy system." *Renewable energy* (2017). *Renewable energy*, vol. 108, pp. 179-193, 2017.
- [28] Q. Sun, D. Xing, H. Alafnan, X. Pei, M. Zhang and W. Yuan, "Design and test of a new two-stage control scheme for SMES-battery hybrid energy storage systems for microgrid applications," *Applied Energy*, vol. 253, p. 113529, 2019.
- [29] M. Elshiekh, M. Zhang, H. Ravindra, X. Chen, S. Venuturumilli, X. Huang, K. Schoder, M. Steurer and W. Yuan, "Effectiveness of Superconducting Fault Current Limiting Transformers in Power Systems," *IEEE Transactions on Applied Superconductivity*, vol. 28, no. 3, pp. 5601607-5601607, 2018.
- [30] F. Liang, et al. "Modeling and experiment of the current limiting performance of a resistive superconducting fault current limiter in the experimental system." *Journal of Superconductivity and Novel Magnetism* 28.9 (2015): 2669-2681.
- [31] Y. Xu, Y. Li, L. Ren, C. Xu, Y. Tang, J. Li, L. Chen and B. Jia, "Research on the Application of Superconducting Magnetic Energy Storage in Microgrids for Smoothing Power Fluctuation Caused by Operation Mode Switching," *IEEE Transactions on Applied Superconductivity*, vol. 28, no. 4, p. 5701306, June 2018. doi: 10.1109/TASC.2018.2808454
- [32] D. M. Yehia, D.-E. A. Mansour and W. Yuan, "Overcurrent and overvoltage testing of a multifunctional superconducting coil," in *2018 53rd International Universities Power Engineering Conference (UPEC)*, Glasgow, Scotland, 2018.
- [33] M. Tsili and S. Papathanassiou, "A review of grid code technical requirements for wind farms," in *IET Renewable Power Generation*, vol. 3, no. 3, pp. 308-332, Sept. 2009. doi: 10.1049/iet-rpg.2008.0070
- [34] S. Wang, C. Li, O. D. Adeuyi, G. Li, C. E. Ugalde-Loo and J. Liang, "Coordination of MMCs With Hybrid DC Circuit Breakers for HVDC Grid Protection," in *IEEE Transactions on Power Delivery*, vol. 34, no. 1, pp. 11-22, Feb. 2019. doi: 10.1109/TPWRD.2018.282870
- [35] H. Chen, J. Yuan, F. Chen and Z. Zhang, "A New Type of Fast-Response Fault Current Limiter topology for HVDC Application," in *IEEE Transactions on Industrial Electronics*, November 2020. doi: 10.1109/TIE.2020.3036217.
- [36] H. Nourmohamadi, M. Nazari-Heris, M. Sabahi and M. Abapour, "A Novel Structure for Bridge-Type Fault Current Limiter: Capacitor-Based Nonsuperconducting FCL," in *IEEE Transactions on Power Electronics*, vol. 33, no. 4, pp. 3044-3051, April 2018, doi: 10.1109/TPEL.2017.2710018
- [37] M. H. Ali, B. Wu and R. A. Dougal, "An Overview of SMES Applications in Power and Energy Systems," in *IEEE Transactions on Sustainable Energy*, vol. 1, no. 1, pp. 38-47, April 2010, doi: 10.1109/TSTE.2010.2044901.
- [38] X. Zhou et al., "Cost Estimation Models of MJ Class HTS Superconducting Magnetic Energy Storage Magnets," in *IEEE Transactions on Applied Superconductivity*, vol. 28, no. 4, pp. 1-5, June 2018, Art no. 5701105, doi: 10.1109/TASC.2018.2821363.
- [39] R. Soman et al., "Preliminary Investigation on Economic Aspects of Superconducting Magnetic Energy Storage (SMES) Systems and High-Temperature Superconducting (HTS) Transformers," in *IEEE Transactions on Applied Superconductivity*, vol. 28, no. 4, pp. 1-5, June 2018, Art no. 5400805, doi: 10.1109/TASC.2018.2817656.
- [40] M. A. Green and B. P. Strauss, "Things to Think About When Estimating the Cost of Magnets Made With Conductors Other Than Nb-Ti," in *IEEE Transactions on Applied Superconductivity*, vol. 27, no. 4, pp. 1-5, June 2017, Art no. 0500305, doi: 10.1109/TASC.2016.2639588.